

# Detection of pure ground-glass nodules in the lung by low-dose multi-detector computed tomography, with use of an iterative reconstruction method: a comparison with conventional image reconstruction by the filtered back-projection method

Shiho Akashita · Yasuhiko Tachibana ·  
Kentarō Sakamaki · Keiji Sogawa · Tomio Inoue

Received: 10 November 2014 / Accepted: 10 December 2014 / Published online: 1 January 2015  
© Japan Radiological Society 2014

## Abstract

**Purpose** To evaluate the feasibility of the iterative reconstruction (IR) method with low-dose multi-detector computed tomography (MDCT) for lung cancer screening.

**Materials and methods** A chest CT phantom containing simulated ground-glass nodules (GGNs) of 5 different sizes was scanned by use of 16-row and 64-row MDCT. Tube currents of 10, 20, and 30 mA were used for the low-dose CT. To assess the detectability of pure GGNs, a radiologist-performance test was conducted. Mean visual scores for simulated GGNs were compared for reconstructed images from filtered back-projection (FBP) and the IR method.

**Results** When 64-row MDCT was used, visual scores for simulated GGNs were significantly higher for the IR method than for the FBP method under any conditions; scores were also significantly higher for 16-row MDCT under some conditions.

**Conclusions** The results of this experimental chest phantom study showed that use of the IR method improved the detectability of simulated pure GGNs.

**Keywords** Adaptive iterative dose reduction · Lung cancer screening test · Low-dose multi-detector computed tomography

## Introduction

The National Lung Screening Trial (NLST) recently reported clinical evidence for lung cancer screening using low-dose helical CT for high-risk examinees. The NLST enrolled approximately 50,000 participants at more than 30 trial sites nationwide over a 20-month period. Participants were required to have a smoking history of at least 30 pack-years and were either current or former smokers without signs, symptoms, or a history of lung cancer. Participants were randomly assigned to be screened annually, three times, with either low-dose helical CT (often referred to as spiral CT) or standard chest X-ray [1]. However, the risk–benefit balance for cancer screening tests by multi-detector computed tomography (MDCT) or chest X-ray must be considered, because radiation exposure is a risk factor that increases the probability of the future development of malignant tumors. The discovery that over-dose radiation exposure as a result of perfusion MDCT resulted in alopecia initiated development of new technology to reduce radiation exposure in MDCT [2, 3].

Image reconstruction by the iterative reconstruction (IR) method is one of the most effective techniques for reducing radiation exposure in MDCT [4–7].

To the best of our knowledge, even though the effectiveness of low-dose MDCT has been proved by using a chest phantom with pure ground-glass nodules (GGNs), detectability by use of low-dose MDCT has not been evaluated quantitatively.

To evaluate the feasibility of the IR method with low-dose MDCT for lung cancer screening, we performed a

S. Akashita (✉) · Y. Tachibana · T. Inoue  
Department of Radiology, Yokohama City Medical College, 3-9,  
Hukuura, Kanazawa, Yokohama, Kanagawa 236-0004, Japan  
e-mail: aka1010star@yahoo.co.jp

K. Sakamaki  
Department of Biostatistics, Yokohama City University, 4-57,  
Urafune, minami, Yokohama, Kanagawa 232-0024, Japan

K. Sogawa  
Yokohama Rosai Hospital, 3211, Kozukue, Kohoku, Yokohama,  
Kanagawa 222-0036, Japan

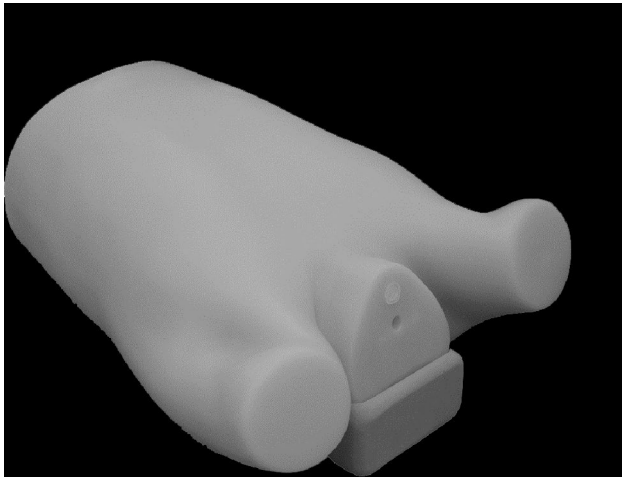


**Fig. 1** Chest CT phantom containing simulated nodules in simulated lungs

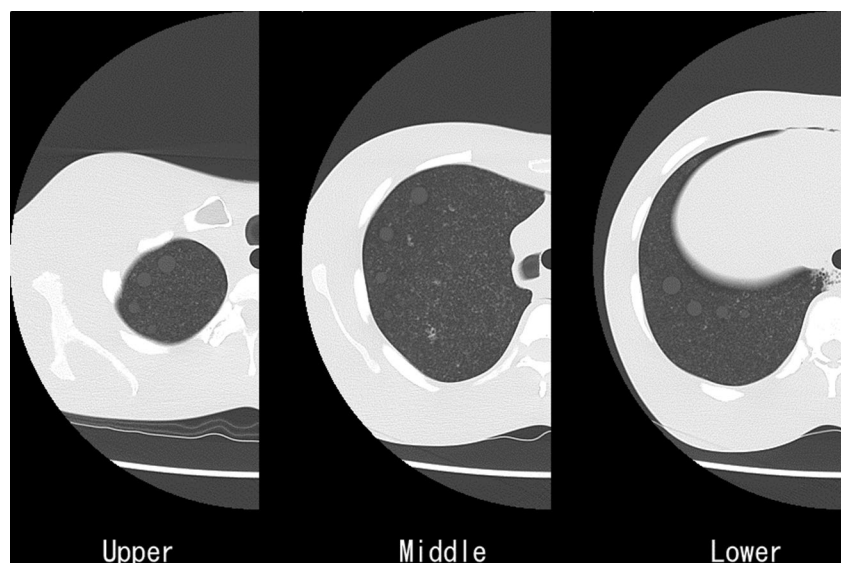
comparative phantom study with conventional image reconstruction by use of the filtered back-projection (FBP) method.

## Materials and methods

### Chest CT phantom

A chest CT phantom (LSCT001; Kyoto Kagaku, Kyoto, Japan) containing simulated nodules in simulated lungs was used. The phantom was a composite of Styrofoam and hard urethane powder in urethane resin adhesive. The simulated tumors were spheres of acrylic foam and urethane in the simulated lung (Fig. 1) [8].

**Fig. 2** Control images. Simulated GGNs with diameters of 4, 6, 8, 10, and 12 mm are seen in the right lung



Details of this device have been reported elsewhere [9]. Simulated GGNs were placed in the right upper portion (lung apex), right middle portion (tracheal bifurcation), and right lower portion (lung base). Simulated solid nodules were placed in the left upper portion (lung apex), left middle portion (tracheal bifurcation), and left lower portion (lung base). The diameters of simulated GGNs placed in the right lung were 4, 6, 8, 10, and 12 mm (Fig. 2).

The CT numbers for the simulated lung, the simulated GGNs, and simulated solid nodules were  $-900$ ,  $-800$  and  $-630$  Hounsfield units (HU), respectively.

### CT scanning

A 16-row MDCT scanner (Alexion; Toshiba Medical Systems, Nasu, Japan) and a 64-row MDCT scanner (Aquilion CXL; Toshiba Medical Systems) were used.

As control images, high-resolution 5-mm images were reconstructed at 5-mm intervals by use of 64-row MDCT scanners operating with the acquisition conditions: tube voltage 120 kVp, scan speed 1.5 s/r, pitch factor 0.641, tube current 350 mA, and detector collimation  $0.5 \times 64$  mm. These conditions resulted in radiation exposure of 99.0 mGy for the volume CT dose index (CTDIvol) and 2,870 mGy/cm for the dose-length product (DLP). The diameters of simulated GGNs placed in the right lung were 4, 6, 8, 10, and 12 mm (Fig. 2).

As subject images, nine different spatial resolution images were used for 16 and 64-row MDCT. The CT acquisition conditions are listed in Tables 1 and 2. In the scan protocol for simulated GGNs, total effective dose (mSv) in 16 and 64-row MDCT ranged from 0.4 to 2.5 and from 0.25 to 1.6, respectively (Tables 1 and 2).

**Table 1** Acquisition conditions for 16-row MDCT

No.	Tube voltage (kV)	Scan speed (s/r)	Detector collimation (mm)	Scan range (mm)	Slice thickness (mm)	Helical pitch	Pitch factor	Tube current (mA)	CTDIvol (mGy)	DLP (mGy cm)	TED (mSv)
1	120	0.75	1.0	300	5	23	1.438	10	0.7	20	0.40
2	120	0.75	1.0	300	5	15	0.938	10	1.1	31	0.61
3	120	0.75	1.0	300	5	11	0.688	10	1.4	42	0.84
4	120	0.75	1.0	300	5	23	1.438	20	1.4	40	0.80
5	120	0.75	1.0	300	5	15	0.938	20	2.1	62	1.20
6	120	0.75	1.0	300	5	11	0.688	20	2.9	84	1.70
7	120	0.75	1.0	300	5	23	1.438	30	2.1	60	1.20
8	120	0.75	1.0	300	5	15	0.938	30	3.2	92	1.80
9	120	0.75	1.0	300	5	11	0.688	30	4.3	126	2.50

*CTDIvol* volume CT dose index, *DLP* dose length product, *TED* total effective dose

**Table 2** Acquisition conditions for 64-row MDCT

No.	Tube voltage (kV)	Scan speed (s/r)	Detector collimation (mm)	Scan range (mm)	Slice thickness (mm)	Helical pitch	Pitch factor	Tube current (mA)	CTDIvol (mGy)	DLP (mGy cm)	TED (mSv)
1	120	0.5	1.0	300	5	45	1.406	10	0.4	12	0.25
2	120	0.5	1.0	300	5	27	0.844	10	0.7	21	0.41
3	120	0.5	1.0	300	5	21	0.656	10	0.9	27	0.53
4	120	0.5	1.0	300	5	45	1.406	20	0.9	25	0.50
5	120	0.5	1.0	300	5	27	0.844	20	1.4	42	0.83
6	120	0.5	1.0	300	5	21	0.656	20	1.8	53	1.10
7	120	0.5	1.0	300	5	45	1.406	30	1.3	37	0.74
8	120	0.5	1.0	300	5	27	0.844	30	2.1	62	1.20
9	120	0.5	1.0	300	5	21	0.656	30	2.8	80	1.60

*CTDIvol* volume CT dose index, *DLP* dose length product; *TED* total effective dose

The nine images of 16 and 64-row MDCT were reconstructed by use of the FBP and IR methods, respectively. In this study, adaptive iterative dose reduction 3D (AIDR 3D) was used as the IR method for MDCT image reconstruction [4–7]. Finally, 36 images were used for the radiologist-performance test for the detectability of simulated GGNs.

**Radiologist-performance test**

A radiologist-performance test was performed to investigate the detectability of the simulated GGNs with different radiation exposure using the two different image-reconstruction methods (FBP and AIDR 3D). In total, eight radiologists in five institutes were asked to participate in this radiologist-performance test using the chest phantom with simulated GGNs in the right lung. The radiologists' experience ranged from 4 to 28 years (mean ± SD, 13.75 ± 9.94 years); five radiologists had <10 years of experience, and three radiologists had >20 years of

experience. The eight radiologists usually read whole body imaging, did not specialize in one region, and read chest CT on a regular basis.

The extracted images were displayed on a black-background and the radiologists interpreted the extracted images on a color monitor with a spatial resolution of 1536 × 2048 (RadiForce GS320; Eizo, Ishikawa, Japan) by use of a Digital Imaging and Communications in Medicine Viewer (RapideyeCore; Toshiba Medical Systems). The attenuation was −900 HU for lung parenchyma and −800 HU for the simulated GGNs.

At the start of the test a control image was presented, and the eight radiologists interpreted the image and confirmed the location, shape, and size of the simulated GGNs, which were clearly visible (Fig. 2).

To assess the detectability of pure GGNs, the visual scores of the eight radiologists who independently interpreted the reconstructed CT images by use of conventional FBP and AIDR 3D methods were evaluated. The

- 5: 100% margin visualized.
- ◐ 4: 51–99% margin visualized
- ◑ 3: 50% margin visualized
- ◒ 2: 1–49% margin visualized
- 1: not visualized

**Fig. 3** Visual scores defined by use of a 5-point scale

radiologists were unaware of the CT acquisition conditions, for example the milliamperage and pitch factor settings, used for acquisition of the image of the phantom. The time for reading the images was not limited. The window width was set at a constant 1,600 HU, and the window level was set at a constant –600 HU for the visual evaluations.

Confidence level was defined by use of a five-point scale:

1. not visualized;
2. 1–49 % of margin visualized;
3. 50 % of margin visualized;
4. 51–99 % of margin visualized; and
5. 100 % of margin visualized (Fig. 3).

To indicate whether or not an object was present, each radiologist placed a score on the recording forms. The images were displayed in a sequence determined by use of a random number table.

#### Statistical analysis

For the eight radiologists, mean visual scores were calculated as the confidence level for detection of simulated GGNs. A paired *t* test was used to evaluate the significance of differences between mean visual scores for detectability by use of the FBP and AIDR 3D methods for reconstructed CT images of simulated GGNs with diameters of 6, 8, and 10 mm in the phantom. Statistical analysis was performed with IBM SPSS Statistics 21 (IBM, Chicago, IL, USA). A

value of  $P < 0.05$  was regarded as indicative of a significant difference.

Before the radiologist-performance test, the location, shape, and size of the simulated GGNs clearly visible on the control images were shown. i.e. true negative and false-positive results were not designed to be part of the experimental procedure, so receiver operating characteristic (ROC) curve analysis could not be conducted.

#### Results

Mean visual scores for simulated pure GGNs were compared between the FBP and AIDR 3D methods for reconstructing CT images at the lowest total effective dose (mSv) when the mean visual score for the AIDR 3D method reached more than 2 (Tables 3 and 4).

With 16-row MDCT, significant differences between mean visual scores for the FBP and AIDR 3D methods were observed for pure GGNs with a diameter of 6 mm in the middle and lower lung fields only and for pure GGNs with a diameter of 10 mm in the upper lung field only (Table 3).

With 64-row MDCT, significant differences between mean visual scores for the FBP and AIDR 3D methods were observed for any location and size, except for pure GGNs with a diameter of 6 mm in the lower lung field only (Table 4).

Representative phantom images in this study are shown in Figs. 4 and 5. Figure 4 shows the 16-row MDCT images reconstructed by use of the FBP and AIDR 3D methods at the lowest total effective dose for visualizing a pure GGN with a diameter of 8 mm. Figure 5 shows the 64-row MDCT images reconstructed by use of the FBP and AIDR 3D methods at the lowest total effective dose for visualizing a pure GGN with a diameter of 6 mm. The lowest total effective dose (mSv) when the mean visual score reached more than 2 is shown in Tables 5, 6.

A pure GGN with a diameter of 6 mm in the upper lung field was not visualized under any of the 16-row MDCT

**Table 3** 16-row MDCT: mean visual scores for simulated pure GGNs by the FBP and AIDR 3D methods at the lowest total effective dose (mSv) when the mean visual score for the AIDR 3D method reached more than 2

	6 mm				8 mm				10 mm			
	TED mSv	FBP mean (SD)	AIDR 3D mean (SD)	<i>P</i> *	TED (mSv)	FBP mean (SD)	AIDR 3D mean (SD)	<i>P</i> *	TED (mSv)	FBP mean (SD)	AIDR 3D mean (SD)	<i>P</i> *
Upper	–	–	–	–	0.61	1.25 (0.46)	2.13 (0.99)	0.087	0.40	1.13 (0.35)	2.63 (1.06)	0.005
Middle	0.4	1.50 (0.93)	2.25 (0.71)	0.020	0.40	2.00 (1.20)	2.25 (0.46)	0.451	0.40	3.13 (1.13)	2.88 (0.83)	0.351
Lower	0.4	1.88 (0.83)	2.75 (0.71)	0.006	0.40	2.38 (0.92)	2.38 (0.92)	1.000	0.40	3.00 (1.07)	3.38 (1.06)	0.351

TED total effective dose, FBP filtered back-projection, AIDR 3D adaptive iterative dose reduction 3D, SD standard deviation

\* A value of  $P < 0.05$  was regarded as indicative of a significant difference



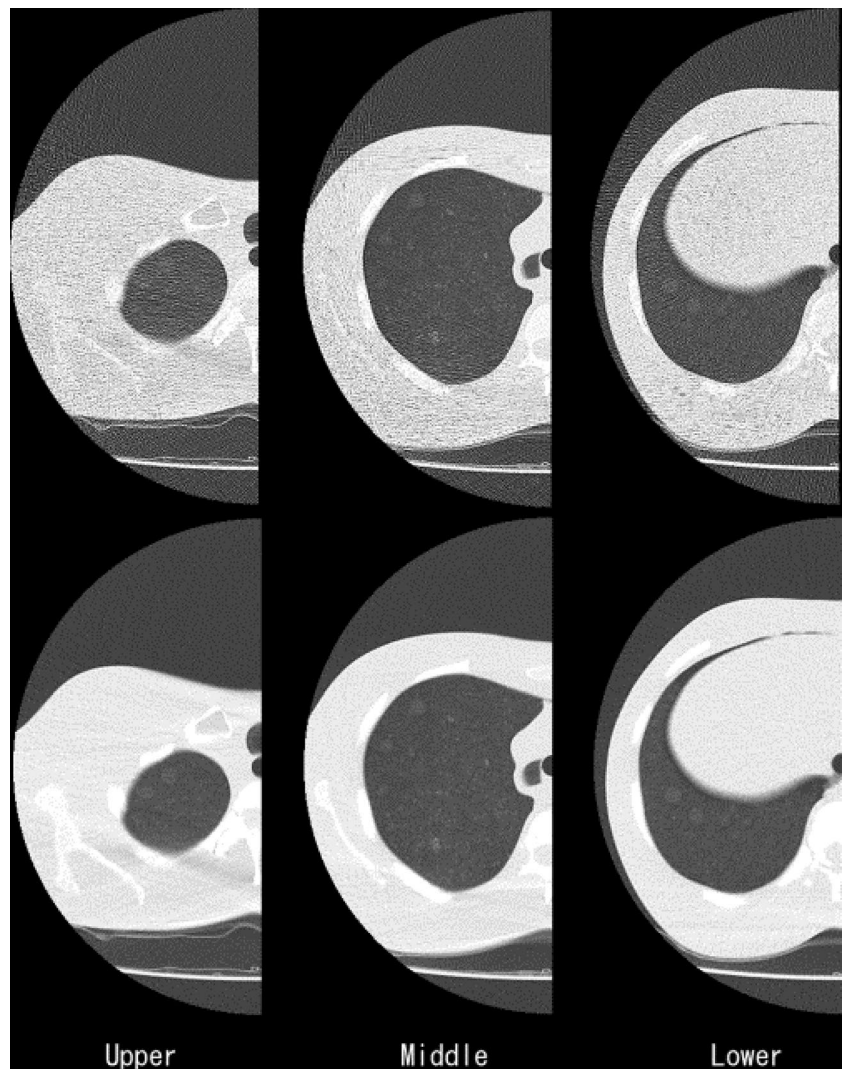
**Table 4** 64-row MDCT: mean visual scores for simulated pure GGNs by the FBP and AIDR 3D methods at the lowest total effective dose (mSv) when the mean visual score for the AIDR 3D method reached more than 2

	6 mm				8 mm				10 mm			
	TED mSv	FBP mean (SD)	AIDR 3D mean (SD)	<i>P</i> *	TED mSv	FBP mean (SD)	AIDR 3D mean (SD)	<i>P</i> *	TED mSv	FBP mean (SD)	AIDR 3D mean (SD)	<i>P</i> *
Upper	0.41	1.13 (0.35)	2.63 (1.19)	0.005	0.25	1.00 (0.00)	2.13 (0.99)	0.015	0.25	1.13 (0.35)	2.25 (1.04)	0.007
Middle	0.41	1.50 (0.76)	3.25 (1.04)	0.002	0.25	2.25 (0.71)	3.38 (0.92)	0.002	0.25	2.63 (0.92)	3.88 (1.13)	0.005
Lower	0.25	1.50 (0.76)	2.25 (1.16)	0.111	0.25	2.25 (0.89)	3.25 (0.89)	0.033	0.25	2.50 (0.76)	3.75 (1.16)	0.019

TED total effective dose, FBP filtered back-projection, AIDR 3D adaptive iterative dose reduction 3D, SD standard deviation

\* A value of *P* < 0.05 was regarded as indicative of a significant difference

**Fig. 4** 16-row MDCT images (10 mA, HP15) reconstructed by use of the FBP and AIDR 3D methods at the lowest total effective dose at which a pure GGN of diameter 8 mm was visualized. The upper images were reconstructed by use of the FBP method and the lower images by use of the AIDR 3D method



acquisition conditions in this study, and a pure GGN with a diameter of 6 mm in the upper lung field was not visualized by the FBP method for reconstructed images for any of the 64-row MDCT acquisition conditions used in this study (these results are presented as blanks in Tables 3, 5, and 6). However, a pure GGN with a diameter of 6 mm in

the upper lung field was visualized by use of the AIDR 3D method for reconstructed images with 64-row MDCT.

For a pure GGN with a diameter of 6 mm, the lowest total effective dose (mSv) was lower with the AIDR 3D method than with the FBP method irrespective of location (Tables 5 and 6). For pure GGNs with diameters of 8 and

**Fig. 5** 64-row MDCT images (10 mA, HP27) reconstructed by use of the FBP and AIDR 3D methods at the lowest total effective dose at which a pure GGN of diameter 6 mm was visualized. The upper images were reconstructed by use of the FBP method and the lower images by use of the AIDR 3D method

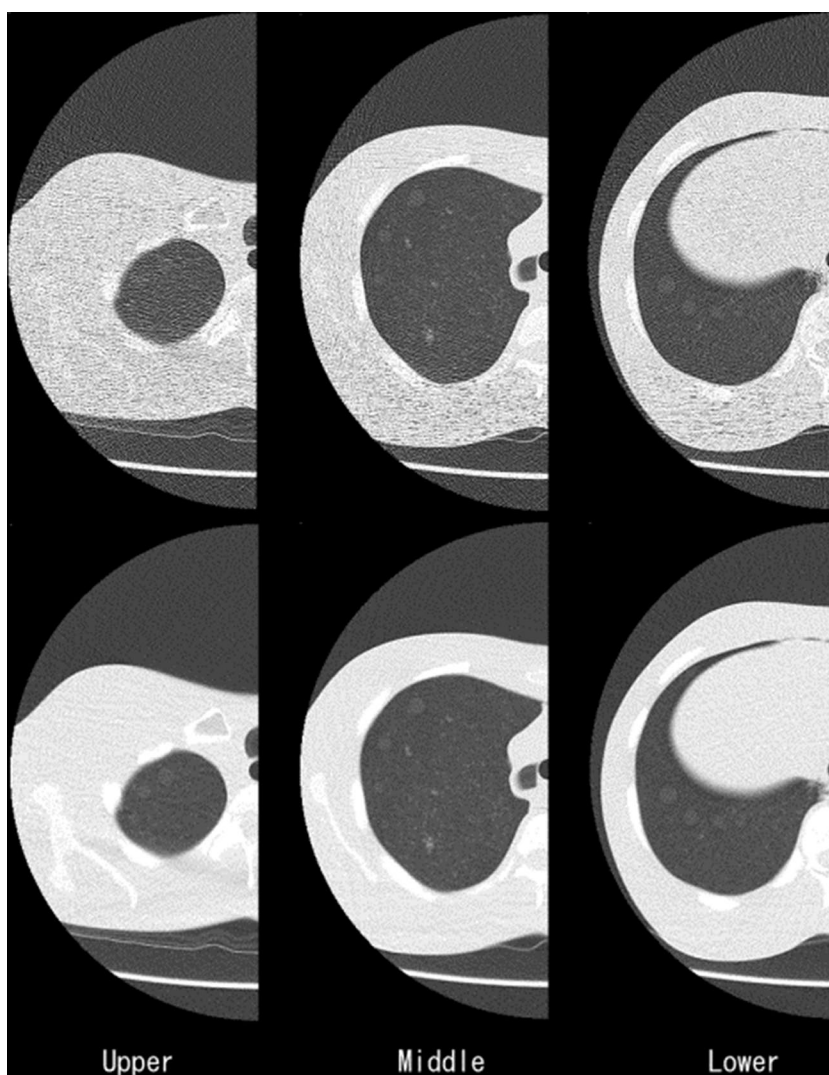


**Table 5** 16-row MDCT: the lowest total effective dose (mSv) when the mean visual score reached more than 2

	6 mm		8 mm		10 mm	
	FBP	AIDR 3D	FBP	AIDR 3D	FBP	AIDR 3D
Upper	–	–	1.20	0.61	0.80	0.40
Middle	0.61	0.40	0.40	0.40	0.40	0.40
Lower	0.61	0.40	0.40	0.40	0.40	0.40

FBP filtered back-projection, AIDR 3D adaptive iterative dose reduction 3D

**Table 6** 64-row MDCT: the lowest total effective dose (mSv) when the mean visual score reached more than 2

	6 mm		8 mm		10 mm	
	FBP	AIDR 3D	FBP	AIDR 3D	FBP	AIDR 3D
Upper	–	0.41	0.74	0.25	0.74	0.25
Middle	0.74	0.41	0.25	0.25	0.25	0.25
Lower	0.41	0.25	0.25	0.25	0.25	0.25

FBP filtered back-projection, AIDR 3D adaptive iterative dose reduction 3D

**Table 7** Mean visual scores for all simulated GGNs with diameters of 6, 8, and 10 mm

16-row MDCT				64-row MDCT			
TED	FBP Mean (SD)	AIDR 3D Mean (SD)	<i>P</i> *	TED	FBP Mean (SD)	AIDR 3D Mean (SD)	<i>P</i> *
0.40	1.89 (1.11)	2.32 (1.00)	<0.001	0.25	1.72 (0.86)	2.65 (1.27)	<0.001
1.20	3.19 (1.40)	3.25 (1.32)	NS	0.74	3.11 (1.19)	3.46 (1.06)	<0.001
2.50	3.56 (1.45)	3.64 (1.42)	NS	1.60	3.54 (1.27)	4.32 (1.27)	<0.001

*TED* total effective dose, *FBP* filtered back-projection, *AIDR 3D* adaptive iterative dose reduction 3D, *SD* standard deviation

\*A value of *P* < 0.05 was regarded as indicative of a significant difference

10 mm, the lowest total effective dose (mSv) was lower for the AIDR 3D method than for the FBP method in the upper lung field only (Tables 5 and 6).

The mean visual scores for all simulated GGNs with diameters of 6, 8, and 10 mm were compared between the FBP and AIDR 3D methods for reconstructing CT images at the minimum, medium, and maximum total effective doses (mSv) (Table 7). For both 16 and 64-row MDCT, the mean visual scores for simulated GGNs were higher with the AIDR 3D method than with the FBP method. At the minimum total effective dose, the mean visual scores with the FBP method were less than 2, but with the AIDR 3D method they were more than 2. At the medium and maximum total effective dose, the mean visual scores with both FBP and AIDR 3D methods were more than 2.

With 16-row MDCT, significant differences between the mean visual scores for the FBP and AIDR 3D methods were observed for the minimum total effective dose only. However, with 64-row MDCT, significant differences between the mean visual scores for the FBP and AIDR 3D methods were observed for any total effective dose.

## Discussion

The National Cancer Institute (NCI) has released initial results from a large-scale test of screening methods performed to reduce deaths from lung cancer. The NLST, a randomized national trial involving more than 50,000 heavy smokers, compared the effects on lung cancer mortality of two screening procedures for lung cancer, low-dose helical computed tomography (CT) and chest X-ray, and found 20 % fewer lung cancer deaths among trial participants screened by low-dose helical CT [1]. The results of the NLST may facilitate lung cancer screening by MDCT. The finding that over-dose radiation exposure by perfusion MDCT resulted in alopecia, however, initiated the development of new technology to reduce radiation exposure by MDCT [2, 3], and several technical trials with auto exposure control (AEC), multiple rows of detectors, and image-based filter techniques have been performed [7, 10, 11]. Recently, a new technique for reducing radiation

exposure, iterative reconstruction, has been used for MDCT image reconstruction. AIDR 3D is one method of iterative reconstruction [4–7]. Considering the risk/benefit balance, especially for health check-ups, the amount of radiation exposure is a significant factor determining its feasibility [12–14].

The extent to which exposure to radiation could be reduced was evaluated by making reconstructed images by use of the AIDR 3D method, a new method with low-dose MDCT. By use of the chest phantom containing simulated GGNs, detectability in reconstructed images was compared between the FBP method and the AIDR 3D method. The nine conditions used for CT acquisition by 16-row MDCT were combinations of tube current 10, 20, or 30 mA and helical pitch, 23, 15, and 11. These resulted in the lowest possible dose for the 16 MDCT scanner to reduce radiation exposure.

In 2000, when MDCTs became available in clinical practice, the 4-row MDCT was a common scanner. After rapid technological innovation over the last 10 years, the row number of MDCT increased to 16. Given this background, 64-row MDCT is likely to become common, which is why 64-row MDCT was investigated with 16-row MDCT in this study.

To investigate the extent to which exposure to radiation could be reduced for lung cancer screening by 64-row MDCT, 9 CT acquisition conditions were chosen: combinations of tube current, 10, 20, or 30 mA; and helical pitch 45, 27, or 21. Again, these resulted in the lowest dose possible for the 64 MDCT scanner to reduce exposure to radiation. Detectability in reconstructed images was compared between the FBP and AIDR 3D methods in the same way as for 16-row MDCT.

A chest phantom has been used in previous experimental studies [8–10]. In this study, simulated GGNs with a diameter of 6 mm were used, because nodules with diameters more than 5 mm are the earliest lung cancers that can be detected by screening, and the smallest of the simulated GGNs in the phantom with a diameter greater than 5 mm were of diameter 6 mm.

A simulated nodule with a diameter of 10 mm simulates another important lesion, because a nodule of diameter more than 5 mm that grows or reaches a diameter of 10 mm

must be confirmed pathologically, either surgically or by obtaining a biopsy specimen [15]. The 8-mm-diameter nodule was selected as a lesion intermediate between the 6 and 10-mm-diameter lesions. This phantom had GGNs in the right lung and solid nodules in the left lung. The GGNs in the right lung were the focus of this study.

Swenson et al. [16] found that nodules were missed in 26 % of patients undergoing their first annual CT examination. GGNs are more difficult to detect than solid nodules; approximately 70 % of lung cancers missed by radiologists during low-dose CT screening were GGNs [17].

Although a GGN is a nonspecific finding that may occur in benign disease, for example focal inflammation, it may be attributable to such malignant lesions as adenocarcinoma in situ (AIS) or minimally invasive adenocarcinoma (MIA). Therefore, reliable detection of GGNs is a critical issue in lung cancer screening with low-dose CT [8].

To increase the objectivity of this study, eight radiologists from five institutes were asked to participate in a radiologist-performance test to investigate the detectability of the simulated GGNs; the test was performed at the same time and under the same conditions and entailed interpretation of images with the same viewer (RapideyeCore; Toshiba Medical Systems). The time allowed for interpretation of the images was not limited.

The images scanned under the 18 different acquisition conditions were reconstructed by use of the FBP and AIDR 3D methods and displayed in a sequence determined by use of a random number table. For quantitative analysis, the visual scores of the eight radiologists who independently interpreted the reconstructed CT images by the conventional FBP method and by the AIDR 3D method were evaluated. The visual scores were defined by use of a five-point scale.

With either 16-row or 64-row MDCT, CT images reconstructed by use of the AIDR 3D method resulted greater detectability of simulated GGNs at the same total effective dose. The simulated GGNs in the upper lung field seemed difficult to identify on reconstructed CT images by the FBP and AIDR 3D methods. It was believed that a bone artefact caused by the ribs near the lung apex interfered with detection. The difference between detectability of GGNs by the FBP and AIDR 3D methods became larger with smaller size and in the upper lung field. When 64-row MDCT was used, simulated GGNs had significantly higher visual scores with the AIDR 3D method than with the FBP method, irrespective of size and location (Tables 3, 4, 5, and 6). To evaluate overall detectability, mean visual scores for all the simulated GGNs with diameters of 6, 8, and 10 mm were compared between the FBP and AIDR 3D methods for reconstructing CT images at the minimum, medium, and maximum total effective dose (mSv) (Table 7). With both 16 and 64-row MDCT, the mean visual

scores for simulated GGNs were higher with the AIDR 3D method than with the FBP method. At the minimum total effective dose, the mean visual scores with the FBP method were less than 2, which means that the radiologists could not detect the GGNs. However, with the AIDR 3D method, the scores were more than 2, which means that the GGNs could be detected. For the medium and maximum total effective dose, the mean visual scores with both FBP and AIDR 3D methods were higher than 2.

With 16-row MDCT, significant differences in the mean visual scores between the FBP and AIDR 3D methods were observed at some conditions. However, with 64-row MDCT, they were observed at any conditions.

These results suggested that when 64-row MDCT is used detectability is better for the AIDR 3D method than for the FBP method, under any conditions; this was also true for 16-row MDCT under some conditions.

One limitation of this study is that it was an experimental phantom study. In clinical lung cancer screening, features that cannot be simulated in a phantom study include:

1. the variety of nodular shape and density;
2. the condition of the background lung parenchyma;
3. breath holding; and
4. motion artefact arising as a result of heart beats, etc.

Further clinical studies are needed to determine CT acquisition conditions suitable for AIDR 3D image reconstruction for lung cancer screening [18].

## Conclusion

The results of this experimental CT study using a chest phantom showed that the IR method contributed to improving the detectability of simulated pure GGNs.

**Acknowledgments** The authors would like to thank F. Suzuki, MD, T. Hara, MD, N. Niiya, MD, H. Fujisawa, MD, J. Watari, MD, and T. Ikegami, MD for their participation in our radiologist-performance test, T. Iinuma, MD, for advice about our study, and M. Taguri, Ph.D. and M. Saito, for statistical analysis. This research was not supported by any external funding.

**Conflict of interest** The authors declare that they have no conflicts of interest.

## References

1. Aberle DR, Adams AM, Berg CD, Black WC, Clapp JD, Fagerstrom RM, et al. Reduces lung-cancer mortality with low-dose computed tomographic screening. *N Engl J Med*. 2011;365:395–409.



2. Riley K. FDA Makes Interim recommendations to address concern of excess radiation exposure during CT perfusion imaging [U.S. Food and Drug Administration Web site]. Dec 7, 2009. Available at: <http://www.fda.gov/NewsEvents/Newsroom/PressAnnouncements/ucm193190.htm>. Accessed 1 July 2013.
3. Imanishi Y, Fukui A, Niimi H, Itho D, Nozaki K, Nakaji S, et al. Radiation-induced temporary hair loss as a radiation damage only occurring in patients who had the combination of MDCT and DSA. *Eur Radiol*. 2005;15:41–6.
4. Yamada Y, Jinzaki M, Hosokawa T, Tanami Y, Sugiura H, Abe T, et al. Dose reduction in chest CT: comparison of the adaptive iterative dose reduction 3D, adaptive iterative dose reduction, and filtered back projection reconstruction techniques. *Eur J Radiol*. 2012;81:4185–95.
5. Tomizawa N, Nojo T, Akahane M, Torigoe R, Kiryu S, Ohtomo K. Adaptive iterative dose reduction in coronary CT angiography using 320-row CT: assessment of radiation dose reduction and image quality. *J Cardiovasc Comput Tomogr*. 2012;6:318–24.
6. Juri H, Matsuki M, Itou Y, Inada Y, Nakai G, Azuma H, et al. Initial experience with adaptive iterative dose reduction 3D to reduce radiation dose in computed tomographic urography. *J Comput Assist Tomogr*. 2013;37:52–7.
7. Yu L, Liu X, Leng S, Kofler JM, Ramirez-Giraldo JC, Qu M, et al. Radiation dose reduction in computed tomography: techniques and future perspective. *Imaging Med*. 2009;1:65–84.
8. Funama Y, Awai K, Liu D, Oda S, Yanaga Y, Nakaura T, et al. Detection of nodules showing Ground-Glass Opacity in the lungs at low-dose multidetector computed tomography: phantom and clinical study. *J Comput Assist Tomogr*. 2009;33:49–53.
9. Muramatsu Y, Tsuda Y, Nakamura Y, Kubo M, Tayama T, Hanai K. The development and use of a chest phantom for optimizing scanning techniques on a variety of low-dose helical computed tomography devices. *J Comput Assist Tomogr*. 2003;27:364–74.
10. Matsumoto K, Ohno Y, Koyama H, Kono A, Inokawa H, Onishi Y, et al. 3D automatic exposure control for 64-detector row CT: radiation dose reduction in chest phantom study. *Eur J Radiol*. 2011;77:522–7.
11. Kubo T, Ohno Y, Gautam S, Lin PP, Kauczor H, Hatabu H. Use of 3D adaptive raw-data filter in CT of the lung: effect on radiation dose reduction. *AJR*. 2008;191:W167–74.
12. Bach PB, Mirkin JN, Oliver TK, Azzoli CG, Berry DA, Brawley OW, et al. Benefits and harms of CT screening for lung cancer. *JAMA*. 2012;307:2418–29.
13. González AB, Darby S. Risk of cancer from diagnostic X-rays: estimates for the UK and 14 other countries. *Lancet*. 2004;363:345–51.
14. Pearce MS, Salotti JA, Little MP, McHugh K, Lee C, Kim KP, et al. Radiation exposure from CT scans in childhood and subsequent risk of leukemia and brain tumours: a retrospective cohort study. *Lancet*. 2012;380:499–505.
15. Nakata M, Saeki H, Takata I, Segawa Y, Mogami H, Mandai K, et al. Focal ground-glass opacity detected by low-dose helical CT. *Chest*. 2002;121:1464–7.
16. Swenson SJ, Jett JR, Sloan JA, Midthun DE, Hartman TE, Sykes A, et al. Screening for lung cancer with low-dose spiral computed tomography. *Am J Respir Crit Care Med*. 2002;165:508–13.
17. Li F, Sone S, Abe H, Macmahon H, Armato G II, Doi K. Lung cancers missed at low – dose helical CT screening in a general population: comparison of clinical, histopathologic, and imaging findings. *Radiology*. 2002;225:673–83.
18. Jaklitsch MT, Jacobson FL, Austin JHM, Field JK, Jett JR, Kes-havjee S, et al. The American Association for Thoracic Surgery guidelines for lung cancer screening using low-dose computed tomography scans for lung cancer survivors and other high-risk groups. *J Thorac Cardiovasc Surg*. 2012;144:33–8.